Comparison of Long-Wave Infrared Imaging and Visible/Near-Infrared Imaging of Vegetation for Detecting Leaking CO_2 Gas

Jennifer E. Johnson, Joseph A. Shaw, *Senior Member*, *IEEE*, Rick L. Lawrence, Paul W. Nugent, Justin A. Hogan, Laura M. Dobeck, and Lee H. Spangler

***Abstract*—Recent research demonstrated that CO_2 gas leaking from underground can be identified by observing increased stress in overlying vegetation using spectral imaging. This has been accomplished with both visible/near-infrared (Vis/NIR) sunlight reflection and long-wave infrared (LWIR) thermal emission. During a 4-week period in summer 2011, a controlled CO_2 release experiment was conducted in Bozeman, Montana, as part of a study of methods for monitoring carbon sequestration facilities. As part of this experiment, reflective and emissive imagers were deployed together to enable a comparison of these two types of imaging systems for vegetation-based CO_2 leak detection. A linear regression was performed using time as the response variable with red and NIR reflectances, Normalized Difference Vegetation Index (NDVI), and LWIR brightness temperature as predictors. The regression study showed that the reflectance and LWIR brightness temperature data together explained the most variability in the data (96%), equal to the performance of the Vis/NIR reflectance data alone, followed by NDVI alone (90%), and LWIR data alone (44%). Therefore, the two types of imagers contributed in a synergistic fashion, while either method alone was capable of gas detection with increased statistical variability.**

***Index Terms*—Environmental monitoring, gas detection, multispectral imaging, thermal imaging.**

Manuscript received June 11, 2013; revised October 10, 2013; accepted November 12, 2013. This paper is based upon work supported in part by the Department of Energy under award number DE-FE0000397. This report was prepared as an account of work sponsored in part by an agency of the United States Government. Neither the United States Government nor any agency thereof, or any of their employees, makes any warranty, expressed or implied, or assumes any legal liability or responsibility for the accuracy, completeness, or usefulness of any information, apparatus, product, or process disclosed, or represents that its use would not infringe privately owned rights. Reference herein to any specific commercial product, process, or service by trade name, trademark, manufacturer, or otherwise does not necessarily constitute or imply its endorsement, recommendation, or favoring by the United States Government or any agency thereof. The views and opinions of authors expressed herein do not necessarily state or reflect those of the United States Government or any agency thereof.

J. E. Johnson, J. A. Shaw, P. W. Nugent, and J. A. Hogan are with Electrical and Computer Engineering Department, Montana State University, Bozeman, MT 59715 USA (e-mail: jshaw@ece.montana.edu).

R. L. Lawrence is with Land Resources and Environmental Sciences Department, Montana State University, Bozeman, MT 59715 USA

L. M. Dobeck is with Energy Research Institute, Montana State University, Bozeman, MT 59715 USA

L. H. Spangler is with Department of Chemistry and Biochemistry, Montana State University, Bozeman, MT 59715 USA

Color versions of one or more of the figures in this paper are available online at http://ieeexplore.ieee.org.

Digital Object Identifier 10.1109/JSTARS.2013.2295760

I. Introduction

GEOLOGIC carbon sequestration is being explored for its potential to reduce emission into the atmosphere of greenhouse gases released in combustion processes [1]–[3]. However, for both safety and effectiveness, sequestration requires reliable methods of monitoring and verifying that the gas remains underground without leaking back into the atmosphere [4], [5]. This is one of the primary objectives being pursued at the Zero Emissions Research and Technology (ZERT) Center at Montana State University (MSU) in Bozeman, Montana. During the summers of 2007–2013, controlled CO_2 release experiments were conducted at an agricultural field west of the MSU campus, where a perforated horizontal well was installed to test CO_2 leak detection methods [6]. Technologies tested during the ZERT experiments included eddy covariance measurements [7], [8], soil conductivity sensing [9], atmospheric tracer plume monitoring [10], inelastic neutron scattering [11], closed-path laser absorption and radon gas measurements [12], [13], open-path laser absorption measurements [14]–[16], *in-situ* visible and near-infrared (Vis/NIR) spectral reflectance measurements of vegetation overlying the well [17], Vis/NIR hyperspectral imaging [18], [19] and multispectral imaging of vegetation [20]–[22], and long-wave infrared (LWIR) thermal imaging of vegetation [23], [24] to identify the location of CO_2 gas leaking from the underground well.

The basic concept driving the use of vegetation imaging to locate leaking CO_2 is that higher soil gas concentrations of CO_2 will stress the vegetation, leading to measurable changes in short-wave reflectance and/or long-wave emission. Higher soil gas concentrations of CO_2 could result in less oxygen and water being drawn from the soil into the plants, resulting in a leaf stomata response and changing the reflectance and radiative properties of the vegetation. The increased plant stress results in increased red reflectance and decreased NIR reflectance [23], [24]. Similar methods have been used with airborne and satellite-based sensors to identify regions of natural CO_2 seepage from Vis/NIR, short-wave infrared, and LWIR images of vegetation and soil [25]–[27]. Some studies have suggested that leaks can be identified through CO_2-induced changes in plant species [28], [29], although most have been based on measuring changes in plant stress. The earlier study by Bateson *et al.* [25] showed that CO_2 gas vents appeared as warm regions in thermal infrared images, and hypothesized that this might be a result of the leaking gas or the soil at the gas vent being warmer than the surrounding vegetation. To these initial hypotheses, our study adds interpretation in terms of plant stress leading to impaired thermoregulation by vegetation, which leads to increased vegetation temperature during day and increased variation in vegetation temperature during day and night [24].

During our experiments at the ZERT facility, Vis/NIR reflectance imaging experiments were initiated in 2008 using a commercial multispectral imager [20], and later continued with a custom-designed, wide-angle imager that uses red and NIR reflective bands [21]–[23]. In comparing measured reflectance values of healthy vegetation to those of vegetation exposed to the leaking CO_2, there were statistically significant temporal and spatial variations in Vis/NIR reflectance and vegetation indices derived from the reflectance. The CO_2 leak location was identified by a more rapid rate of plant stress relative to the usual seasonal decay in the control regions.

During the summer 2011 controlled release experiment, we also deployed a LWIR imager to measure vegetation stress and thereby indirectly identify the gas leak location from thermal emission [23], [24]. The mechanism was expected to be essentially the same, but in this case, the stress caused by high soil gas concentrations of CO_2 at the plant roots was hypothesized to result in an impairment of the vegetation's temperature regulation. A consequence of this was that over time, the vegetation nearest to the leak exhibited larger diurnal temperature variations and, most significantly, higher maximum daytime brightness temperatures (temperature of an ideal blackbody emitting the same amount of radiation, equal to the physical temperature when the object is an ideal blackbody).

The side-by-side deployment of reflective and emissive imagers in the summer 2011 experiment enabled a direct comparison of these two remote sensing instruments for locating a CO_2 gas leak through optical signatures of induced vegetation stress. This paper reports the results of this comparison, showing that the data from the two types of imagers are statistically significant alone and provide a moderate level of synergy when combined. The LWIR imager can be deployed without an in-field calibration source, giving it a practical advantage, especially for aerial monitoring of large areas.

II. Methods

The vegetation imagers were mounted on a 3-m scaffold, looking down at approximately 45° onto a vegetation test area (Fig. 1). The horizontal well, buried at a nominal depth of 2 m, ran just in front of the scaffold, across the bottom of the images. The released CO_2 exited the ground in a highly nonuniform pattern [6], [30]–[32], creating localized regions of elevated CO_2 concentrations that we refer to as "hot spots." The 2011 release ran from July 18 to August 15, 2011, with a flow rate of 0.15 tons/day. Images were acquired once per minute throughout daylight hours for the reflective imager and throughout both day and night for the emissive imager. Images were analyzed in a hot spot region known to have high CO_2 flux and two control regions with near background-level CO_2 flux (Fig. 2). The use of two control regions allowed us to find that there is no substantial view-angle dependence in the results [23], [24].

Fig. 1. Side-by-side Vis/NIR and LWIR imagers mounted on a scaffold to measure vegetation reflectance and emission, respectively, at the ZERT field in Bozeman, Montana. The tripod in front of the scaffold is a mount that holds a reflectance panel to calibrate the Vis/NIR images.

The reflective imager has 1280×1024 pixels and custom front-end optics that provide wide-angle imaging through interference filters mounted in a rotating filter wheel. The filters have 40-nm half-power bandwidths, centered at 800 nm for the NIR channel and 630 nm for the red channel [21]. The reflective imager has an embedded computer that runs custom software to control the instrument. During this deployment, red and NIR image pairs were acquired once each minute. A Spectralon 99%-reflectance panel was deployed on a tripod mount in the midst of the vegetation test area, so that it was included in a portion of each image. A laboratory calibration was used to relate the pixels in that particular portion of each image to all of the pixels throughout the image, resulting in a calibration that converted digital numbers to reflectance. From these reflectance data, Normalized Difference Vegetation Index (NDVI) values were calculated from (1), and then the 1-min reflectance and NDVI data in the hot spot and two control regions were averaged from 10 AM to 2 PM (when the Sun is sufficiently high to reduce shadows in the vegetation) to create a single value of red reflectance, NIR reflectance, and NDVI for each region on each day

$$NDVI = \frac{\mathrm{NIR} - \mathrm{Red}}{\mathrm{NIR} + \mathrm{Red}}. \quad (1)$$

Note that the NDVI is a nonindependent interaction term for red and NIR reflectance [33], which has been shown in previous studies to have substantial statistical explanatory effect [20]–[22], [33].

The LWIR imager was mounted on the same scaffold, immediately beside the reflective imager (Fig. 1). The FLIR photon 320 LWIR camera with 320×240 pixels produced 14-bit digital images, whose digital numbers were calibrated using a method developed at Montana State University for maintaining radiometric calibration even with widely varying camera temperature and no calibration target in the field [34]. The resulting values of

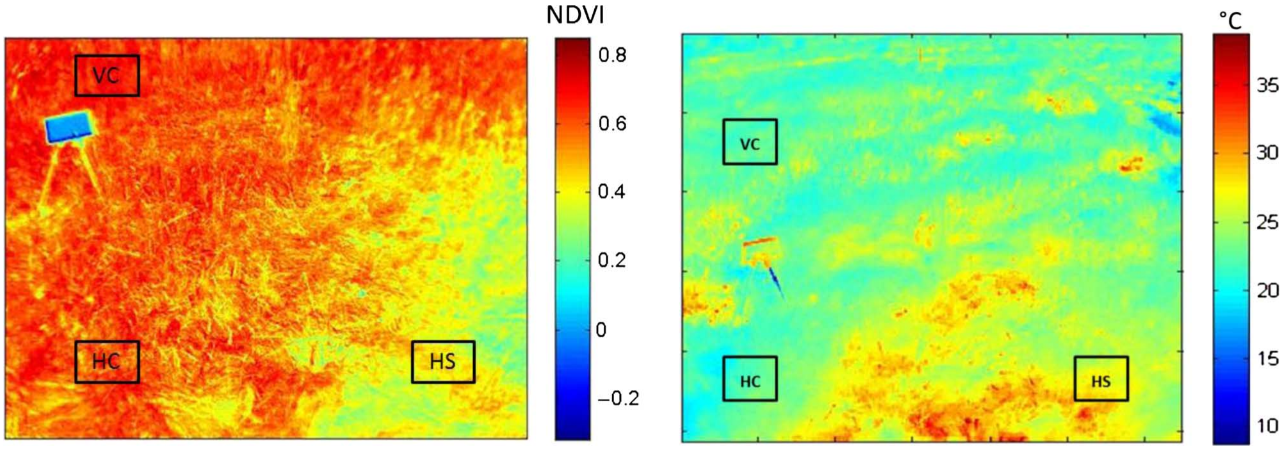

Fig. 2. Approximate locations of the hot spot (HS), horizontal control (HC), and vertical control (VC) regions shown on images of the vegetation test area from 14 August 2011: (left) NDVI and (right) LWIR brightness temperature in °C.

radiance $[\mathrm{W}/(\mathrm{m}^2 \cdot \mathrm{sr})]$ at each pixel were converted to brightness temperature (T_b), in °C, with a lookup table computed by integrating the product of the Planck blackbody function and the 8- to $14\text{-}\mu\mathrm{m}$ spectral response function of the imager. The T_b values in all the thermal images were spatially averaged within the hot spot region and the two control regions to produce a time series of region-average T_b.

III. Comparison of Reflective and Emissive Images

To facilitate a statistical comparison of the performance of the two types of imagers during the 2011 CO_2 release experiment, linear regressions were calculated using DAY (number of days since the start of operation with side-by-side imagers) as the response variable and reflectance, NDVI, and T_b as predictors. We used DAY as the response variable because although DAY does not respond to the spectral responses, it enables comparison of the correlations between DAY and spectral responses even when there are multiple spectral responses being tested in a single regression. Furthermore, DAY acts as a surrogate for exposure level to the constantly flowing CO_2 gas, which is the biophysical driver of the response we were measuring.

This procedure was similar to the analysis implemented in prior years for the reflective data alone [20]–[22], but this iteration added thermal brightness temperature data and the second control region. Thermal images were acquired during day and night, starting in early June 2011, whereas reflective images were acquired only during day, starting in early July 2011. Although the extra images acquired prior to the start of the release and during hours other than at midday increased the amount of variance explained by the thermal data [23], [24], the comparison reported here uses images only from midday (10 AM–2 PM) on the common days when both the reflective and emissive imagers were operating together (14 July–23 August 2011, with gas flowing from 18 July to 15 August).

We began the analysis by performing separate linear regressions on NDVI data alone, red and NIR data alone, and thermal brightness temperature data alone to determine whether each of these data types by itself was able to produce statistically significant results that allowed us to distinguish between the hot spot and control regions [23]. The linear regression model for the NDVI was formulated as follows:

$$\mathrm{DAY} = \beta_0 + \beta_1 \mathrm{NDVI} + \beta_2 \mathrm{REGION} + (\beta_3 \mathrm{NDVI} \times \mathrm{REGION}). \tag{2}$$

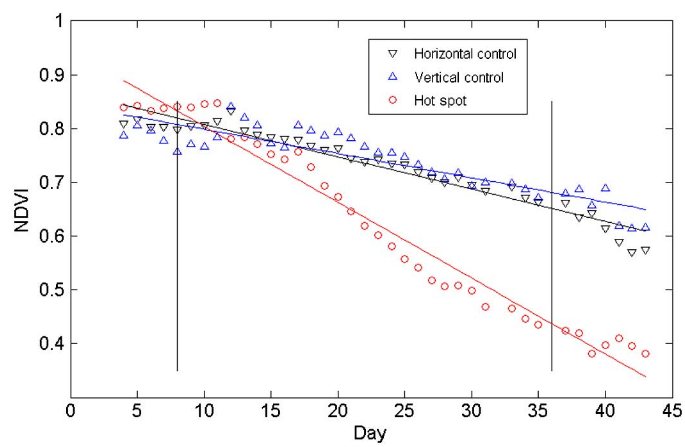

Fig. 3. NDVI versus day of the experiment plotted for three test regions. The vertical lines mark the start and end of the CO_2 gas release on 18 July and 15 August 2011, respectively.

In (2), DAY is the response variable representing the number of days elapsed since the start of operation for both side-by-side imagers, REGION is a categorical variable that selects from the three regions of interest (hot spot, horizontal control, or vertical control), and the β terms are the regression coefficients. We created a reduced model by removing terms that were not found to be statistically significant, starting with the least significant term. Statistical significance was determined by a term having a p-value less than or equal to 0.05 (the p-value is the probability of observing a sample statistic that is as extreme as the test statistic). The reduced model for the NDVI regression (3) resulted in a residual standard error of 3.76 on 109 degrees of freedom, with an adjusted R^2 value of 0.90

$$\begin{aligned}\mathrm{DAY} = {} & 144.47 - 164.19\,\mathrm{NDVI} - 1.71\,\mathrm{VC} - 78.91\,\mathrm{HS} \\ & + (95.61\,\mathrm{NDVI} \times \mathrm{HS}).\end{aligned} \tag{3}$$

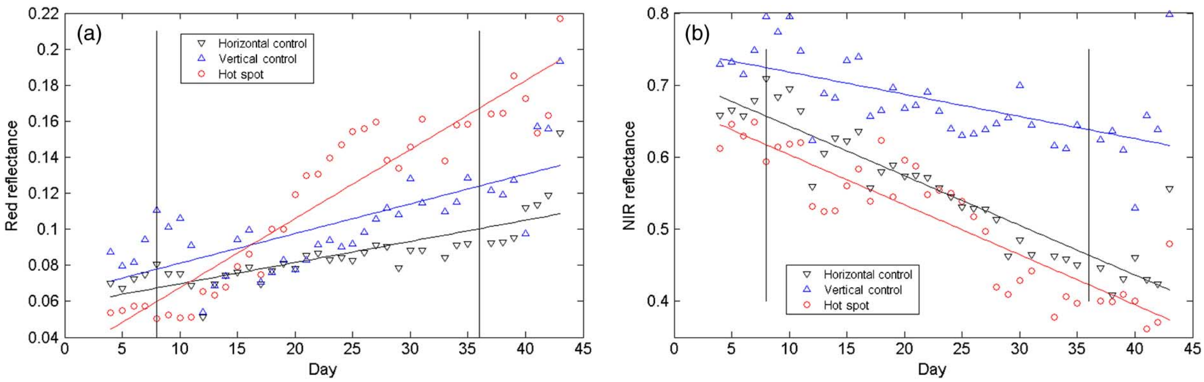

Fig. 4. Reflectance versus day of the experiment plotted for all three test regions: (left) red and (right) NIR.

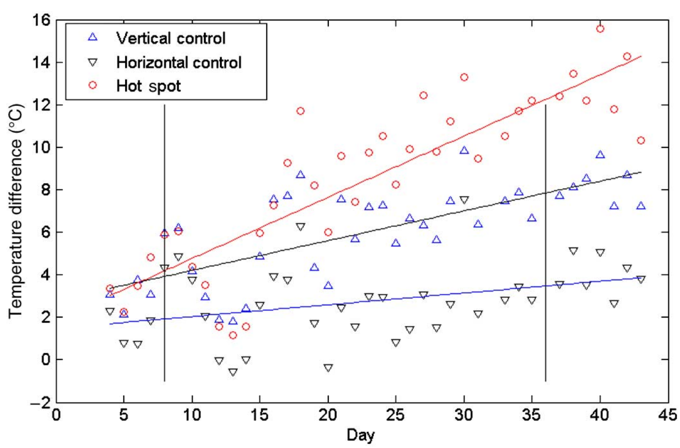

Fig. 5. Plot showing difference in LWIR brightness temperature and air temperature versus day of the experiment for the three test regions.

In (3), VC and HS are the values of the categorical variable REGION, representing the vertical control or hot spot regions, respectively. In this case, both regions were compared with the horizontal control region in the regression; i.e., for observations in VC, $\mathrm{VC}=1$ and $\mathrm{HS}=0$, for observations in HS, $\mathrm{VC}=0$ and $\mathrm{HS}=1$, and for observations in HC, $\mathrm{VC}=0$ and $\mathrm{HS}=0$. This enables three possible models, depending on the value of VC and HS. The three models are represented by the three regression lines shown in Figs. 3–5.

These results show that there was a statistically significant difference between the vertical control and hot spot regions. The coefficient estimated for the hot spot intercept was substantially larger than the coefficient for the vertical control intercept, meaning the hot spot had a much greater difference from the horizontal control than the vertical control, which was quite similar to the horizontal control.

Fig. 3 is a time-series plot of daily average NDVI plotted with time on the horizontal axis for convenience (although to interpret the regression values in the table, it is important to keep in mind that the regressions were actually performed with experiment day as the response variable). The vertical lines indicate the start and end of the CO_2 release. This figure shows that the NDVI data from all three regions started out similar, but decayed with different rates for the control and hot spot regions after the onset of the CO_2 release. The similarity of the curves from the two control regions indicates that there is no substantial view-angle difference in the data. As expected, the NDVI data from the hot spot region decayed at a much higher rate than in either control region.

A similar linear regression was calculated for the red and NIR reflectance data

$$\begin{aligned}\mathrm{DAY} = {} & \beta_0 + \beta_1\mathrm{NIR} + \beta_2\mathrm{RED} + \beta_3\mathrm{REGION} \\ & + (\beta_4\mathrm{NIR}^*\mathrm{REGION}) + (\beta_5\mathrm{RED}\times\mathrm{REGION}). \qquad (4)\end{aligned}$$

Again, a reduced model was obtained by eliminating terms that were found to not have statistical significance according to the requirement that p-value ≤ 0.05. This regression gave a residual standard error of 2.39 on 106 degrees of freedom with an adjusted R^2 value of 0.96. The reduced reflectance regression model is shown in (5), and the reflectance versus experiment day is plotted in Fig. 4. The temporal trends were as expected, with the red reflectance rising and the NIR reflectance falling as the vegetation dried out through the summer, but with the highest rate of change in the hot spot region because of the additional stress caused by the high soil gas concentration. It is interesting to note the similarity in the slope of the hot spot and vertical control lines for the NIR reflectance in Fig. 4. The NIR reflectance is primarily responsive to leaf structure, but the lack of biophysical measurements prevents us from interpreting this with confidence

$$\begin{aligned}\mathrm{DAY} = {} & 75.66 - 126.65\,\mathrm{NIR} + 323.92\,\mathrm{RED} - 30.94\,\mathrm{VC} \\ & - 42.05\,\mathrm{HS} + 37.64(\mathrm{NIR}\times\mathrm{VC}) + 71.34(\mathrm{NIR}\times\mathrm{HS}) \\ & - 172.57(\mathrm{RED}\times\mathrm{HS}). \qquad (5)\end{aligned}$$

The same type of analysis was performed on the infrared brightness temperatures for the days when both imagers were operating together. To isolate the plant health-related thermal signature from the meteorological variations, the ambient air temperature was subtracted from the infrared brightness temperature for all readings. The full linear regression model for the emissive thermal image data used the same REGION categorical variable as our previous models, along with a ΔT term representing the difference of IR brightness temperature and air temperature ($\Delta T = T_b - T_a$), as follows:

$$\mathrm{DAY} = \beta_0 + \beta_1\mathrm{REGION} + \beta_2\Delta T + \beta_3(\Delta T\times\mathrm{REGION}). \qquad (6)$$

The reduced ΔT regression model in (7) resulted in a residual standard error of 8.71 on 110 degrees of freedom with an adjusted R^2 value of 0.44. Again, the temporal trend shown in Fig. 5 was as expected, with ΔT increasing as the vegetation became stressed while summer progressed, but with the highest rate of increase in the hot spot region

$$\mathrm{DAY}=6.03-6.95\mathrm{HS}+9.18\mathrm{VC}+2.81\Delta T. \quad (7)$$

The trend shown in Fig. 5 arose because ΔT increased as the stressed vegetation lost its ability to regulate its own temperature, resulting eventually in an IR T_b that was higher than the ambient air temperature because of solar heating during the day. The vegetation nearest to the hot spot region showed markedly higher ΔT values than the unexposed vegetation. In this case, the difference between the slopes of the regression lines for the two control regions was slightly significant, indicating that there is no substantial concern with view angle. Note that the plant–air temperature difference ΔT has been shown previously to carry information related to plant water stress; specifically, for a well-irrigated crop, the temperature difference was shown to start out slightly negative because evapotranspiration cooled the sunlit plants below the ambient air temperature, and increasing water stress caused the temperature difference to pass through zero and then become increasingly positive as the plants progressively lost their ability to regulate their own temperature [35].

Having shown that both the Vis/NIR imager data and the LWIR imager data independently yielded statistically significant results, we next combined the NDVI, reflectance, and brightness temperature data into the following single regression model:

$$\begin{aligned}\mathrm{DAY} = {} & \beta_0 + \beta_1\mathrm{NDVI} + \beta_2\mathrm{NIR} + \beta_3\mathrm{RED} + \beta_4\Delta T \\ & + \beta_5\mathrm{REGION} + \beta_6(\mathrm{NDVI}\times\mathrm{REGION}) \\ & + \beta_7(\mathrm{NIR}\times\mathrm{REGION}) + \beta_8(\mathrm{RED}\times\mathrm{REGION}) \\ & + \beta_9(\Delta T\times\mathrm{REGION}). \end{aligned} \quad (8)$$

The full-model reduced regression in (9) resulted in a residual standard error of 2.24 on 103 degrees of freedom with an adjusted R^2 value of 0.96

$$\begin{aligned}\mathrm{DAY} = {} & 1.02 + 66.73\,\mathrm{NDVI} - 120.75\,\mathrm{NIR} + 469.2\,\mathrm{RED} \\ & + 0.13\Delta T + 66.34\,\mathrm{HS} + 26.15\,\mathrm{VC} \\ & - 129.81(\mathrm{NDVI}\times\mathrm{HS}) + 109.90(\mathrm{NIR}\times\mathrm{HS}) \\ & - 30.20(\mathrm{NIR}\times\mathrm{VC}) - 475.03(\mathrm{RED}\times\mathrm{HS}). \end{aligned} \quad (9)$$

This full regression model using combined reflective and emissive data shows that the reflectance, NDVI, and thermal infrared measurements are all significant for identifying CO_2-affected regions from unaffected regions of vegetation. The individual regressions [(3), (5), and (7)] also are each strong by themselves, indicating that a CO_2-affected region can be identified by one method alone (reflectance, NDVI, or LWIR emission). The highest R^2 value (0.96) occurred for both the reflectance regression and the combined reflective-and-emissive regression. This suggests that the most effective single type of measurement may be Vis/NIR reflectance, although there is statistically significant value in measuring both reflectance and emission.

IV. Conclusion

Through comparison of the regression results, it is evident that the emissive data combine in a statistically significant manner with the reflectance-band data. However, either reflective or emissive imaging alone can distinguish between regions with and without a CO_2 leak. Nevertheless, in the manner that the imagers were deployed in our experiment, the LWIR imaging method was simplest because it did not require a reflectance calibration panel in the field, only air temperature data, which are generally readily available. Thus, if this method was used for airborne monitoring, thermal imaging would require deployment of air temperature sensors in the area being monitored (along with the use of an appropriate model to compensate for atmospheric emission and attenuation), while Vis/NIR imaging would require either field deployment of a sufficiently large reflectance calibration panel, deployment of downwelling solar irradiance sensors in the field, or use of other calibration methods that allow the images to be processed for reflectance (along with appropriate compensation for atmospheric scattering and attenuation). Finally, the use of two control regions in this analysis shows that there is no substantial concern over viewing angle. Continuing work includes testing imagers from balloons or aircraft to allow viewing of larger areas. In practical use, this method suggests that elevated LWIR brightness temperatures relative to ambient air temperature or rapidly changing Vis/NIR reflectance could indicate a potential leak for which final confirmation could be made using ground-based measurements.

References

[1] J. D. Figueroa, T. Fout, S. Plasynski, H. McIlvried, and R. D. Srivastava, "Advances in CO_2 capture technology—The U.S. Department of Energy's Carbon Sequestration Program," *Int. J. Greenhouse Gas Contr.*, vol. 2, no. 1, pp. 9–20, 2008.

[2] H. Yang, Z. Xu, M. Fan, R. Gupta, R. B. Slimane, A. E. Bland, and I. Wright, "Progress in carbon dioxide capture and separation: A review," *J. Environ. Sci.*, vol. 20, no. 1, pp. 14–27, 2008.

[3] S. J. Friedmann, "Geological carbon dioxide sequestration," *Elements*, vol. 3, no. 3, pp. 179–184, 2007.

[4] C. M. Oldenburg and A. J. A. Unger, "On leakage and seepage from geologic carbon sequestration sites: Unsaturated zone attenuation," *Vadose Zone J.*, vol. 2, no. 3, pp. 287–296, 2003.

[5] C. M. Oldenburg, J. L. Lewicki, and R. P. Hepple, "Near-surface monitoring strategies for geologic carbon dioxide storage verification," Lawrence Berkeley National Lab Report, 2003 [Online]. Available: http://escholarship.org/uc/item/1cg241jb.

[6] L. H. Spangler, L. M. Dobeck, K. S. Repasky, A. R. Nehrir, S. D. Humphries, J. L. Barr, C. J. Keith, J. A. Shaw, J. H. Rouse, A. B. Cunningham, S. M. Benson, C. M. Oldenburg, J. L. Lewicki, A. W. Wells, J. R. Diehl, B. R. Strazisar, J. E. Fessenden, T. A. Rahn, J. E. Amonette, J. L. Barr, W. L. Pickles, J. D. Jacobson, E. A. Silver, E. J. Male, H. W. Rauch, K. S. Gullickson, R. Trautz, Y. Kharaka, J. Birkholzer, and L. Wielopolski, "A shallow subsurface controlled release facility in Bozeman, Montana, USA, for testing near surface CO_2 detection techniques," *Environ. Earth Sci.*, vol. 60, no. 2, pp. 227–239, 2010.

[7] J. L. Lewicki, G. E. Hilley, M. L. Fischer, L. Pana, C. M. Oldenburg, L. M. Dobeck, and L. H. Spangler, "Detection of CO_2 leakage by eddy covariance during the ZERT project's CO_2 release experiments," *Energy Procedia*, vol. 1, no. 1, pp. 2301–2306, 2009.

[8] J. L. Lewicki and G. E. Hilley, “Eddy covariance network design for mapping and quantification of surface CO_2 leakage fluxes,” *Int. J. Greenhouse Gas Contr.*, vol. 7, pp. 137–144, 2012.
[9] X. Zhou, V. R. Lakkaraju, M. Apple, L. M. Dobeck, K. Gullickson, J. A. Shaw, A. B. Cunningham, L. Wielopolski, and L. H. Spangler, “Experimental observation of signature changes in bulk soil electrical conductivity in response to engineered surface CO_2 leakage,” *Int. J. Greenhouse Gas Contr.*, vol. 7, pp. 20–29, 2012.
[10] A. Wells, B. Strazisar, J. R. Diehl, and G. Veloski, “Atmospheric tracer monitoring and surface plume development at the ZERT pilot test in Bozeman, Montana, USA,” *Environ. Earth Sci.*, vol. 60, no. 2, pp. 299–305, 2010.
[11] L. Wielopolski and S. Mitra, “Near-surface soil carbon detection for monitoring CO_2 seepage from a geological reservoir,” *Environ. Earth Sci.*, vol. 60, no. 2, pp. 307–312, 2010.
[12] J. E. Fessenden, S. M. Clegg, T. A. Rahn, S. D. Humphries, and W. S. Baldridge, “Novel MVA tools to track CO_2 seepage, tested at the ZERT controlled release site in Bozeman, MT,” *Environ. Earth Sci.*, vol. 60, no. 2, pp. 325–334, 2010.
[13] I. McAlexander, G. H. Rau, J. Liem, T. Owano, R. Fellers, D. Baer, and M. Gupta, “Deployment of a carbon isotope ratiometer for the monitoring of CO_2 sequestration leakage,” *Anal. Chem.*, vol. 83, pp. 6223–6229, 2011.
[14] S. D. Humphries, A. R. Nehrir, C. J. Keith, K. S. Repasky, L. M. Dobeck, J. L. Carlsten, and L. H. Spangler, “Testing carbon sequestration site monitor instruments using a controlled carbon dioxide release facility,” *Appl. Opt.*, vol. 47, no. 4, pp. 548–555, 2008.
[15] J. L. Barr, S. D. Humphries, A. R. Nehrir, K. S. Repasky, L. M. Dobeck, J. L. Carlsten, and L. H. Spangler, “Laser-based carbon dioxide monitoring instrument testing during a 30-day controlled underground carbon release field experiment,” *Int. J. Greenhouse Gas Contr.*, vol. 5, no. 1, pp. 138–145, 2011.
[16] W. Johnson, K. S. Repasky, and J. L. Carlsten, “Micropulse differential absorption lidar for identification of carbon sequestration site leakage,” *Appl. Opt.*, vol. 52, no. 13, pp. 2994–3003, 2013.
[17] E. J. Male, W. L. Pickles, E. A. Silver, G. D. Hoffmann, J. L. Lewicki, M. Apple, K. S. Repasky, and E. A. Burton, “Using hyperspectral plant signatures for CO_2 leak detection during the 2008 ZERT CO_2 sequestration field experiment in Bozeman, Montana,” *Environ. Earth Sci.*, vol. 60, no. 2, pp. 251–261, 2010.
[18] C. J. Keith, K. S. Repasky, R. L. Lawrence, S. C. Jay, and J. L. Carlsten, “Monitoring effects of a controlled subsurface carbon dioxide release on vegetation using a hyperspectral imager,” *Int. J. Greenhouse Gas Control*, vol. 3, no. 5, pp. 626–632, 2009.
[19] G. J. Bellante, S. L. Powell, R. L. Lawrence, K. S. Repasky, and T. A. O. Dougher, “Aerial detection of a simulated CO_2 leak from a geologic sequestration site using hyperspectral imagery,” *Int. J. Greenhouse Gas Control*, vol. 13, pp. 124–137, 2013.
[20] J. H. Rouse, J. A. Shaw, R. L. Lawrence, J. L. Lewicki, L. M. Dobeck, K. S. Repasky, and L. H. Spangler, “Multi-spectral imaging of vegetation for detecting CO_2 leaking from underground,” *Environ. Earth Sci.*, vol. 60, no. 2, pp. 313–323, 2010.
[21] J. A. Hogan, J. A. Shaw, R. L. Lawrence, and R. M. Larimer, “Low-cost multispectral vegetation imaging system for detecting leaking CO_2 gas,” *Appl. Opt.*, vol. 51, no. 4, pp. 59–66, 2012.
[22] J. A. Hogan, J. A. Shaw, R. L. Lawrence, J. L. Lewicki, L. M. Dobeck, and L. H. Spangler, “Detection of leaking CO_2 gas with vegetation reflectances measured by a low-cost multispectral imager,” *IEEE J. Sel. Top. Appl. Earth Obs. Remote Sens.*, vol. 5, no. 3, pp. 699–706, Jun. 2012.
[23] J. E. Johnson, “Remote sensing applications of uncooled long-wave infrared thermal imagers,” M.S. thesis, Dept. Electric. Comput. Eng., Montana State Univ., Bozeman, MT, 2012 [Online]. Available: http://scholarworks.montana.edu/xmlui/handle/1/1573.
[24] J. E. Johnson, J. A. Shaw, R. L. Lawrence, P. W. Nugent, L. M. Dobeck, and L. H. Spangler, “Long-wave infrared imaging of vegetation for detecting leaking CO_2 gas,” *J. Appl. Remote Sens.*, vol. 6, p. 063612-1, 2012. DOI: 10.1117/1.JRS.6.063612.
[25] L. Bateson, M. Vellico, S. E. Beaubien, J. M. Pearce, A. Annunziatellis, G. Ciotoli, F. Coren, S. Lombardi, and S. Marsh, “The application of remote-sensing techniques to monitor CO_2-storage sites for surface leakage: Method development and testing at Latera (Italy) where naturally produced CO_2 is leaking to the atmosphere,” *Int. J. Greenhouse Gas Contr.*, vol. 2, pp. 388–400, 2008.
[26] R. Govindan, A. Korre, S. Durucan, and C. E. Imrie, “A geostatistical and probabilistic spectral image processing methodology for monitoring potential CO_2 leakages on the surface,” *Int. J. Greenhouse Gas Contr.,* 2010. DOI: 10.1016/j.ijggc.2010.04.014.
[27] R. Govindan, A. Korre, S. Durucan, and C. E. Imrie, “Comparative assessment of the performance of airborne and spaceborne spectral data for monitoring surface CO_2 leakages,” *Energy Procedia*, vol. 4, pp. 3421–3427, 2011.
[28] M. Krüger, J. West, J. Frerichs, B. Oppermann, M. C. Dictor, C. Joulian, D. Jones, P. Coombs, K. Green, J. Pearce, F. May, and I. Moller, “Ecosystem effects of elevated CO_2 concentrations on microbial populations at a terrestrial CO_2 vent at Laacher See, Germany,” *Energy Procedia*, vol. 1, pp. 1933–1939, 2009.
[29] R. R. P. Noble, L. Stalker, S. A. Wakelin, B. Pejcic, M. I. Leybourne, A. L. Hortle, and K. Michael, “Biological monitoring for carbon capture and storage—A review and potential future developments,” *Int. J. Greenhouse Gas Contr.*, vol. 10, pp. 520–535, 2012.
[30] C. M. Oldenburg, J. L. Lewicki, L. Pan, L. M. Dobeck, and L. H. Spangler, “Origin of the patchy emission pattern at the ZERT CO_2 release site,” *Environ. Earth Sci.*, vol. 60, no. 2, pp. 241–250, 2010.
[31] J. L. Lewicki, G. E. Hilley, M. L. Fischer, L. Pan, C. M. Oldenburg, L. Dobeck, and L. Spangler, “Detection of CO_2 leakage by eddy covariance during the ZERT project’s CO_2 release experiments,” *Energy Procedia*, vol. 1, pp. 2301–2306, 2009.
[32] J. L. Lewicki, C. M. Oldenburg, L. Dobeck, and L. H. Spangler, “Surface CO_2 leakage during the first shallow subsurface CO_2 release experiment,” Lawrence Berkeley National Laboratory Report, 2008 [Online]. Available: http://escholarship.org/uc/item/44g635nc.
[33] R. L. Lawrence and W. J. Ripple, “Comparisons among vegetation indices and bandwise regression in a highly disturbed, heterogeneous landscape: Mount St. Helens, Washington,” *Remote Sens. Environ.*, vol. 64, no. 1, pp. 91–102, 1998.
[34] P. W. Nugent, J. A. Shaw, and S. Piazzolla, “Correcting for focal plane array temperature dependence in microbolometer infrared cameras lacking thermal stabilization,” *Opt. Eng.*, vol. 52, no. 6 2013 DOI: 10.1117/1.OE.52.6.061302.
[35] R. D. Jackson, R. J. Reginato, and S. B. Idso, “Wheat canopy temperature: A practical tool for evaluating water requirements,” *Water Resour. Res.*, vol. 13, no. 3, pp. 651–656, 1977.

Jennifer E. Johnson received the Bachelor’s degree in mechanical engineering and the Master’s degree in electrical engineering from Montana State University, Bozeman, MT, USA, in 2009 and 2012, respectively.

The focus of her research is remote sensing applications of uncooled long-wave infrared imagers and analysis of multispectral remote sensing data.

Joseph A. Shaw (S’84–M’90–SM’04) received the B.S. degree in electrical engineering from the University of Alaska, Fairbanks, AK, USA, the M.S. degree in electrical engineering from the University of Utah, Salt Lake City, UT, USA, and the M.S. and Ph.D. degrees in optical sciences from the University of Arizona, Tucson, AZ, USA, in 1987, 1989, 1994, and 1996, respectively.

From 1989 to 2001, he was an Electro-Optical Engineer at the National Oceanic and Atmospheric Administration (NOAA) Environmental Technology Laboratory, Boulder, CO, USA, where he developed infrared spectroradiometers and laser sensors for studying the Earth’s atmosphere and oceans. In 2001, he joined the electrical and computer engineering faculty at Montana State University, Bozeman, MT, USA, where he is now Professor and Director of the Optical Technology Center. His current research is in polarimetric and radiometric imaging and laser remote sensing.

Dr. Shaw is a Fellow of the Optical Society of America (OSA) and the International Society of Optics and Photonics (SPIE). Professional recognition of his contributions to optical remote sensing science, engineering, and education include the Presidential Early Career Award for Scientists and Engineers (PECASE), the Vaisala Award from the World Meteorological Organization, and the Cox Family Award for Excellence in Scholarship and Teaching at Montana State University.

Rick L. Lawrence received the B.A. degree in political science from Claremont McKenna College, Claremont, CA, USA, the J.D. degree from Columbia University School of Law, New York, NY, USA, and the M.S. and Ph.D. degrees in forest resources from Oregon State University, Corvallis, OR, USA, in 1976, 1979, 1995, and 1998, respectively.

He practiced law from 1979 to 1993 with the law firms or Hughes, Hubbard, & Reed Adams, Duque, and Hazeltine, and LeBoeuf, Lamb, Leiby, & McCrea. He joined the Land Resources and Environmental Sciences Faculty at Montana State University, Bozeman, MT, USA, where he is now Professor and Director of the Spatial Sciences Center. His research spans a wide range of applications related to natural resource management, from carbon sequestration, to crop and range issues, and to forest and wildlife. He also has a strong interest in algorithm development for classification of remotely sensed imagery and specializing in classification tree analysis and its variants.

Dr. Lawrence is a Member of the American Society of Photogrammetry and Remote Sensing, the Society of American Foresters, the American Geophysical Union, and the California Bar Association (inactive).

Paul W. Nugent received the B.S. and M.S. degrees in electrical engineering from Montana State University, Bozeman, MT, USA, in 2005 and 2008, respectively.

Currently, he is a Research Engineer with the Electrical and Computer Engineering Department, Montana State University and President of NWB Sensors Inc., Bozeman, MT, USA. His research activities include radiometric thermal imaging and optical remote sensing.

Justin A. Hogan received the Bachelor's degree in electrical engineering with a supplemental major in applied mathematics from New Mexico State University, Las Cruces, NM, USA, in 2008 and the Master of Science degree in electrical engineering from Montana State University, Bozeman, MT, USA, in 2011, where he is a Doctoral Student in the Electrical and Computer Engineering Department, Montana State University.

He works with the radiation tolerant computing group as a Graduate Research Assistant in Montana State University. His research interests include embedded system design and development, radiation tolerant computing system research, and FPGA system design.

Laura M. Dobeck received the B.S. degree in chemistry from the University of Wisconsin-Madison, WI, USA, in 1991, and the M.S. and Ph.D. degrees in physical chemistry from Cornell University, Ithaca, NY, in 1994 and 1999, respectively.

She has studied reaction dynamics of small molecules in the gas phase using laser spectroscopy and electron transfer in the solution phase with ultrafast laser systems. Her current interests include studying the transport of CO_2 in the near ground surface and testing and evaluating surface and near-subsurface monitoring techniques to be applied to geological carbon dioxide sequestration. She currently serves as the Field Site Manager for the ZERT shallow subsurface CO_2 controlled release facility at Montana State University, Bozeman, MT, USA.

Dr. Dobeck is a Member of the American Geophysical Union (AGU).

Lee H. Spangler received the B.A. degree from Washington & Jefferson College, Washington, PA, USA, in 1980, and the Ph.D. degree in physical chemistry at the University of Pittsburgh, Pittsburgh, PA, in 1985.

From 1985 to 1987, he was a Postdoctoral Researcher with Los Alamos National Laboratory, Los Alamos, NM, USA. He joined the chemistry faculty with Montana State University in 1987, where he now serves as the Director of the Energy Research Institute and Associate Vice President for research.